PCCP

Check for updates

Substrate-induced enhancement of the chemical reactivity in metal-supported graphene

Carlos Romero-Muñiz, [iD] [a] Ana Martín-Recio, [b] Pablo Pou, [ac] José M. Gómez-Rodríguez [iD] *[bcd] and Rubén Pérez [iD] *[ac]

Graphene is commonly regarded as an inert material. However, it is well known that the presence of defects or substitutional hetero-atoms confers graphene promising catalytic properties. In this work, we use first-principles calculations to show that it is also possible to enhance the chemical reactivity of a graphene layer by simply growing it on an appropriate substrate. Our comprehensive study demonstrates that, in strongly interacting substrates like Rh(111), graphene adopts highly rippled structures that exhibit areas with distinctive chemical behaviors. According to the local coupling with the substrate, we find areas with markedly different adsorption, dissociation and diffusion pathways for both molecular and atomic oxygen, including a significant change in the nature of the adsorbed molecular and dissociated states, and a dramatic reduction ($\sim$60%) of the O_2 dissociation energy barrier with respect to free-standing graphene. Our results show that the graphene–metal interaction represents an additional and powerful handle to tailor the graphene chemical properties with potential applications to nano patterning, graphene functionalization and sensing devices.

1 Introduction

The extensive research accumulated since the discovery of graphene has systematically demonstrated its exceptional properties. Many of them arise from the existence of massless conduction electrons near the Fermi level[1] leading to extremely high electron mobilities[2,3] and unique electronic properties.[4] In addition, it possesses the highest thermal conductivity,[5] excellent optical properties,[6] and it is the strongest material ever tested.[7] However, graphene displays a poor chemical reactivity that may be an obstacle for certain target applications like graphene functionalization, the production of two-dimensional covalent nanopatterns or the use of graphene membranes as catalysts. For the last issue, it is true that the controlled incorporation of different defects[8] and especially substitutional heteroatoms like nitrogen[9] are able to induce a remarkable chemical reactivity. In this work, we propose an easier way to enhance the chemical reactivity of a graphene layer by simply considering the interaction with a strongly interacting substrate like Rh(111). This induced reactivity

will not rise G/Rh(111) as a new competitive catalyst, unlike the metallic substrate, a really good catalytic material by itself. The aim of this work is not the search for a new catalyst but to demonstrate that it is possible to selectively enhance the chemical reactivity in certain areas of the graphene layer by a simple, straightforward procedure.

The growth of graphene on transition metal surfaces by Chemical Vapor Deposition (CVD) has proved to be an economic and very efficient choice[10–15] among the different synthetic routes for graphene production.[16,17] Furthermore, the wide selection of different substrates available[18,19] allows the possibility of an additional refinement of graphene corrugation and electronic properties. While in the case of weakly interacting substrates, like Au(111),[20] Cu(111)[12,21] or Pt(111),[11,22] the G layer remains flat and the Dirac cones are preserved (except for a rigid shift due to the charge transfer), for strongly interacting metals, including Ru(0001),[14] Rh(111)[13,23] or Re(0001),[24] the metal substrate induces a significant corrugation in the graphene layer, as large as $\sim$1 Å, and the electronic properties of pristine graphene are completely altered, loosing the characteristic linear dispersion of the Dirac cones as a consequence of the strong hybridization with the substrate. Note also, the existence of intermediate cases like Ir(111)[10] or Pd(111).[25]

According to this scenario, our proposal consists in taking advantage of the influence of the substrate in the global properties of the system, instead of considering it as a mere support to make growth possible. In particular, we demonstrate how the G–metal interaction can be used to enhance the overall

[a] *Departamento de Física Teórica de la Materia Condensada, Universidad Autónoma de Madrid, E-28049 Madrid, Spain. E-mail: ruben.perez@uam.es*

[b] *Departamento de Física de la Materia Condensada, Universidad Autónoma de Madrid, E-28049, Madrid, Spain. E-mail: josem.gomez@uam.es*

[c] *Condensed Matter Physics Center (IFIMAC), Universidad Autónoma de Madrid, E-28049 Madrid, Spain*

[d] *Instituto Nicolás Cabrera, Universidad Autónoma de Madrid, E-28049 Madrid, Spain*

chemical reactivity of the graphene layer, and especially in those areas where the hybridization degree is higher. Due to the strong interaction, the G–Rh distance varies significantly (~ 1 Å) within the moiré unit cell.[13] This large corrugation, that modulates the interaction and confers distinctive chemical and electronic properties to the high and low areas of the moiré, has profound implications on the chemical behavior of adsorbed species.

In this work, we make a comprehensive characterization of the adsorption of molecular and atomic oxygen on the G/Rh(111) interface, including also the diffusion of atomic oxygen over the graphene layer. Our results reveal that the distinctive features found for the adsorption and diffusion of oxygen species follow the G–Rh interaction along the moiré unit cell. Moreover, the electronic structure calculations point out that the most favorable adsorption sites are governed by the local arrangement of carbon atoms with respect to the metallic substrate. Most reactive sites present a higher local density of states near the Fermi level, induced by the substrate, which facilitates changes in the hybridization state of the carbon. Finally, we study the reaction mechanisms for the molecular oxygen dissociation directly on the G–metal system. The total energy barrier for this process is clearly reduced by the presence of the substrate especially in the lowest areas of the moiré pattern, which somehow resemble the catalytic properties of bare metal surfaces. In these more reactive areas the oxygen molecule chemisorbs on the graphene leading to a dissociation path rather different to the one observed for free-standing graphene and favoring the existence of the dissociated species. Therefore, this analysis demonstrates that the surface reactivity can be increased by the presence of the substrate without introducing defects or other extrinsic agents. These conclusions are not exclusively restricted to the case of Rh. A similar behavior is expected for other strongly interacting substrates like Ru(0001) or Re(0001), and even for intermediate cases like Ir(111) and Pd(111).

2 Computational details

Our theoretical approach is based on Density Functional Theory (DFT) calculations using the plane-wave basis code VASP[26] with a cutoff of 400 eV for the basis set. Pseudopotentials for all species were built using the PAW method.[27,28] A Generalized Gradient Approximation was used for the exchange and correlation functional as described by Perdew, Burke and Ernzerhof (PBE-functional)[29] with the D2 semi-empirical correction[30] to take into account dispersion forces. This point is especially relevant to reproduce the proper values of corrugations.[23,31] Spin polarization is required in all calculations involving the O_2 molecule or isolated oxygen atoms, due to its paramagnetic behavior, while we tested that it is not necessary for chemisorbed atomic oxygen.

We use the lattice parameters of graphene and rhodium obtained with DFT calculations (3.7729 Å for bulk Rh, 2.6678 Å in Rh(111), and 2.4678 Å for G, 1.4248 Å in the C–C distance).

All these values are very close to their corresponding experimental counterparts (3.80 Å for bulk rhodium[32] and 1.42 Å for the C–C distance in G[4]). Periodic boundary conditions are used in the simulations with different unit cells. The calculations are performed on a unit cell constituted by a $\left[(\sqrt{43} \times \sqrt{43})\text{-}R7.6^\circ\right]_G$ G layer on a four-layer Rh(111) slab with a $(6 \times 6)_{Rh}$ periodicity. This rhombic unit cell has a side of 16.17 Å and more than 14 Å of vertical spacing are left between periodical images along the z axis. This unit cell (containing 86 C atoms, 144 Rh atoms and the oxygen atoms) reproduces the main features of the large $\left[(12 \times 12)\text{-}R0^\circ\right]_G$ moiré commonly found in the experiments and, thanks to its smaller size, makes the DFT study feasible. The procedure to build these commensurate cells taking into account the residual mismatch between the two lattices is not trivial and it has been explained in detail in a previous work.[13] In this unit cell, the strain in the graphene layer is only -0.04%.

All structures were subjected to ionic relaxations following a conjugate gradient algorithm until forces upon atoms were less than 0.01 eV Å^{-1}. During these relaxations, the two deepest layers of the slab were kept fixed in their bulk positions while all the rest, including oxygen atoms, were allowed to relax. The reciprocal space was sampled using a $2 \times 2 \times 1$ Monkhorst–Pack grid[33] during the structural relaxation, while a thinner grid $11 \times 11 \times 1$ was employed for electronic structure calculations.

Finally, the Climbing Image Nudged Elastic Band (CI-NEB) method[34] has been used to determine the energy barriers both in the diffusion processes and in the molecular oxygen dissociation. In these calculations the convergence criterion in forces was lowered to 0.05 eV Å^{-1} and the spring constant between images was set to 1.5 eV Å^{-2}. Five intermediate images have been used in the diffusion barriers and seven (in two out of three cases) for the complex dissociation paths.

3 Results and discussion

3.1 Adsorption and diffusion of atomic oxygen on G/Rh(111)

The adsorption and diffusion of atomic oxygen on free-standing graphene has been studied by first principles calculations[35] showing that: (i) it adsorbs on bridge G positions, and (ii) diffusion takes place following a bridge–top–bridge path. The calculated energy barrier was 0.73 eV[35] (our calculation yields 0.74 eV), and the transition state, with oxygen on a top position, shows the carbon atom with a sp^3 hybridization. This energy barrier allows the oxygen diffusion over G even at room temperature (with a jump rate of 1 Hz, assuming an attempt frequency of 10^{13} Hz).

In this section, we want to show how the adsorption and diffusion of atomic oxygen are modulated by the G–metal distance in the moiré pattern. In the highest parts, where the G–metal distance is larger (~ 3 Å) and the interaction weaker, the adsorption takes place in the same way as it occurs on pristine graphene. The oxygen atoms form a triangle with two C–O covalent bonds of 1.46 Å characteristic of epoxy groups (see left panel of Fig. 1). On the other hand, in the low parts,
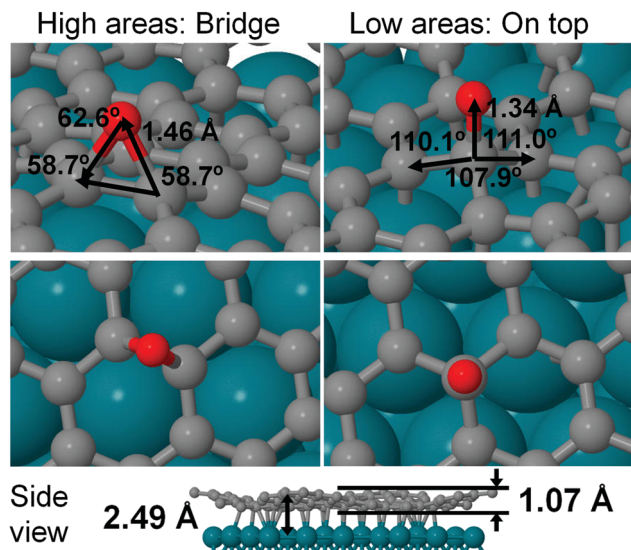
Fig. 1 Different adsorption configurations of atomic oxygen on G/Rh(111). In the highest moiré areas the bridge positions are the most energetically favorable like in free-standing graphene, while in the lowest zones of the moiré the adsorption occurs on top positions. In the lower panel a side view of the interface is shown indicating the values of corrugation and adsorption distance. In all cases Rh atoms are represented in blue, C atoms in grey and O atoms in red.
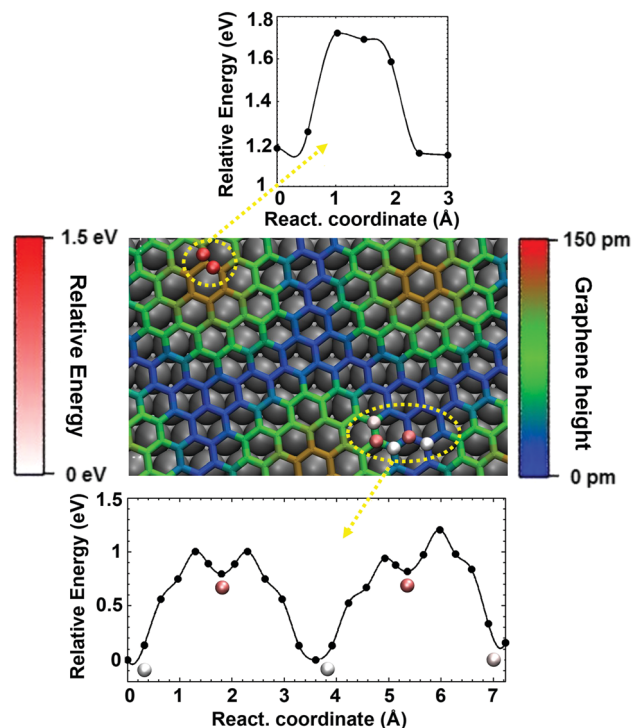

Fig. 2 Diffusion paths for atomic oxygen on the G/Rh(111) surface calculated with CI-NEB. Notice how the diffusion in the top parts (left), energetically less favorable, occurs like in free-standing G following bridge–top–bridge paths, while in the lower parts (right) diffusion takes place jumping from top to top positions. In the central panel, the blue-green-red color scale displays the relative height of the carbon atoms on G/Rh(111) prior to O deposition, while the white-red color of the spheres represents the relative adsorption energy of the oxygen atom on that particular site (taking the most stable O adsorption configuration as reference). Rhodium atoms are depicted as grey spheres.

which are closer to the metallic substrate, the interaction is stronger and bridge positions become unstable. In those areas, adsorption occurs by placing oxygen atoms right on top positions as it is shown in the right panel of Fig. 1. Notice that both adsorptions configurations (bridge and top) described before are strongly chemisorbed to the G/Rh(111) interface as it is revealed by the calculated geometries and adsorption energies. Either in high or low areas the final adsorbed state is several eV more energetically favorable than the detached state far away from the interface, leading to adsorption energies of −2.52 eV and −3.79 eV respectively. Furthermore, due to this great stability, no other adsorption configurations are available in this interface. For instance, simulations started from other, *a priori*, feasible sites (*e.g.* center of the ring) leads to the discussed on-top or bridge configurations without finding any energy barrier.

Something similar occurs if we analyze the diffusion process, where again it is necessary to distinguish between the high and low areas of the moiré pattern. We find, similarly to the adsorption case, that the diffusion path on free-standing graphene is reproduced in the higher moiré parts. Bridge positions are the most energetically favorable adsorption sites and the transition state is close, although not exactly, at top position. However, a difference is found in the diffusion energy barrier that is reduced to 0.55 eV (see upper panel of Fig. 2). On the contrary, the diffusion path is significantly different in the low moiré areas where some top positions are the most favorable O adsorption sites. Due to the interaction with the metal, not all C atoms are equivalent: those located right on top of Rh atoms have larger O adsorption energies, ~0.8 eV more, than C atoms arranged on hollow Rh sites. The transition state is now close to a bridge

position, so the diffusion follows a top–bridge–top path. The total energy barrier is ~1 eV (see central and lower panels of Fig. 2). Notice that, despite these larger values for the diffusion barriers with respect to the high moiré areas, the adsorption in the low areas is significantly more favorable (by ~1.2 eV). Thus, oxygen adsorption and diffusion on G/Rh(111) takes place mainly in the areas more attached to the metal surface. The low values obtained for the activation energies allow fast diffusion of oxygen atoms over the G layer at a broad range of temperatures below the graphene etching temperature (~570 K).[36,37]

We have shown how in the G/Rh(111) interface there are different regions with clearly distinguishable chemical behavior. It is clear that these differences arise from the modulation of the graphene coupling with the substrate along the moiré unit cell resulting in areas with similar properties of free-standing graphene and more reactive areas with different features. However, this fact does not explain the surprising nonequivalent properties of C atoms belonging to the lowest parts, as revealed by the acute differences in adsorption energies presented in the lower panel of Fig. 2. From the energetic point of view, adsorption on certain sites of the low areas is preferred. Notice also that, in the low areas, different adsorption sites are not equivalent despite having very similar G–metal distances.
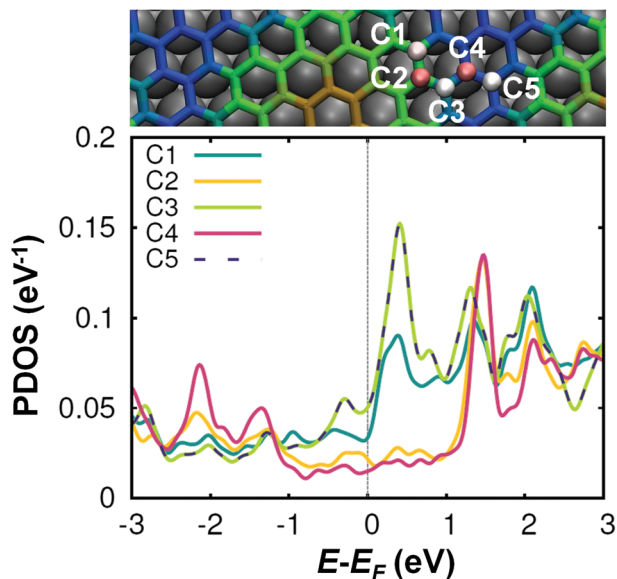
Fig. 3 Projected density of states for five carbon atoms of the low moiré area revealing different chemical behaviors for oxygen adsorption depending on the location with respect to the metallic surface. Each carbon atom is indicated in the lower panel (with the same color code of Fig. 2), just below the adsorbed oxygen atom. Notice how most favorable adsorption configurations correspond to those atoms with a higher number of accessible states near the Fermi level.

The reason of this asymmetry is related to the orientation of the G layer with respect to the metallic surface. Oxygen adsorption on those carbon atoms placed near hollow positions (with respect to the metal) are clearly more favorable (0.5–1 eV) than on others located near top positions, yielding similar adsorption energies to the ones in the highest zones of the moiré pattern. This change in the adsorption behavior is provoked by the interaction with the metallic substrate, which alters the electronic properties of the closest carbon atoms. Fig. 3 shows the Projected Density of States (PDOS) of C atoms corresponding to five adsorption sites. This result suggests that, unlike the common assumption, the electronic properties of

C atoms do not only depend on the moiré area but also on the local arrangement of C atoms with respect to the metallic ones. In such a way that even two nearest-neighbor carbon atoms show remarkable differences in the electronic properties, and thus, reactivity (for example C4 compared to C3 or C5). As it can be seen the most favorable sites display a notorious peak in the PDOS near the Fermi level, which is responsible for a higher chemical reactivity compared to other close atoms. Therefore, the main effect of the G–Rh interaction on the electronic properties of the G is the hybridization of the G-π band with the d rhodium orbitals.[23,38] This interaction is stronger in the C atoms just on top of the Rh atoms. Consequently, the neighbouring C atoms have softened its sp^2 hybridization, and, in the presence of a reactive species like atomic oxygen, these atoms prefer to form a stronger covalent bond with the oxygen by changing to an sp^3 hybridization. This is confirmed by the bond angles of 109.5°, very close to the ideal tetrahedral value, shown in Fig. 1.

3.2 Molecular oxygen dissociation

In this section, we study the dissociation process of molecular oxygen on the G/Rh(111) surface. It is well-known that molecular oxygen and other small molecules easily dissociate on transition metal surfaces. We checked this fact by computing the dissociation barrier of the O_2 molecule on bare Rh(111) which is 0.26 eV, in very good agreement with previous calculations.[39] Moreover, this decomposition reaction is strongly exothermic with a difference in energy of −3.32 eV per molecule. As expected, these results indicate that molecular oxygen tends to dissociate on the catalytic surface of Rh(111) and atomic species prevail. However, this is not the case on free-standing graphene, where molecular oxygen would not be able to dissociate, as reported in previous studies.[40]

Fig. 4 summarizes the results of this section showing the dissociation paths for the O_2 molecule on different substrates obtained with the CI-NEB approach. The dissociation barrier on free-standing graphene is 3.03 eV (Fig. 4a) which is too high to allow dissociation in typical experimental conditions.
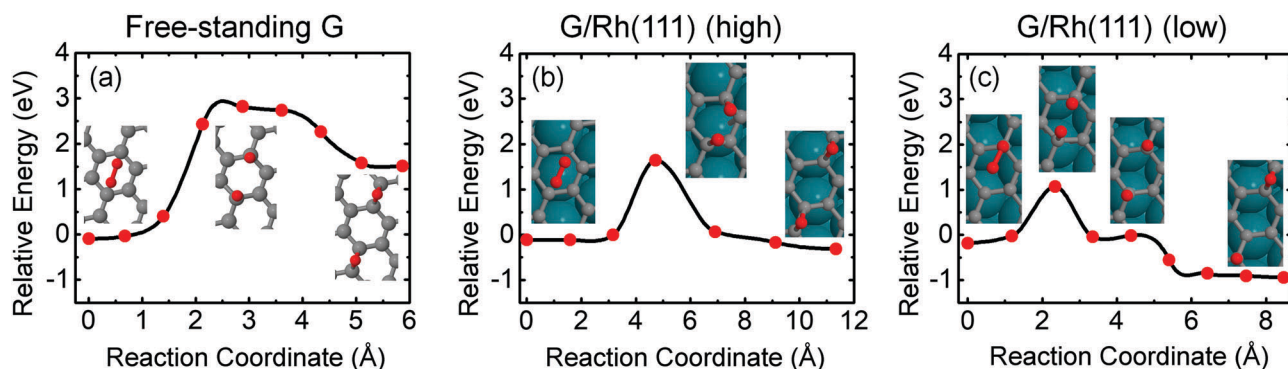

Fig. 4 Dissociation energy barriers for the O_2 molecule on different substrates obtained with CI-NEB. (a) Free-standing graphene, (b) G/Rh(111) on the top moiré area, (c) G/Rh(111) on the low moiré area. Red dots represent the final energy of the NEB images while the black lines are cubic spline interpolations. The insets show schematic top views of the initial state of the adsorbed molecule, the final stage with two oxygen atoms, and the transition states of maximum energy. Notice the remarkable difference in behavior between the top and low areas of the moiré pattern. Energies are referred to the isolate G/Rh(111) slab and O_2 molecule. The color code is as follows: blue (Rh atoms), gray (C atoms) and red (O atoms).

This journal is © the Owner Societies 2018

Phys. Chem. Chem. Phys., 2018, 20, 19492–19499 | 19495

Furthermore, the molecular state is more stable by $\sim$1.5 eV than the dissociated one, making the reaction strongly endothermic. However, the scenario becomes quite different in the presence of the Rh metallic surface underneath G. Again, we have to consider separately the high areas of the moiré, where the G–metal interaction is smaller, and those low areas where the layer is more strongly attached to the metal. In the high areas, showed in Fig. 4b, the adsorption configuration and the dissociation path are very similar to the one in free-standing graphene. Nevertheless, the nature of the interaction with G has already changed significantly, leading to an energy barrier of 1.76 eV. Although this value is still high to allow dissociation, the reaction becomes exothermic, with the dissociated atoms being slightly more stable than the molecular state. Surprisingly, in the low areas of the moiré pattern, the adsorption and dissociation processes are completely different. The dissociation path (Fig. 4c) shows an energy barrier of only 1.25 eV which could be overcome at moderate temperatures ($\sim$500 K), leading to oxygen dissociation directly on the G layer (again, a process rate of 1 Hz and an attempt frequency of 10^{13} Hz). The key to understand these changes in the molecular adsorption and the considerable reduction in the energy barrier is the same discussed in the previous section. In the low G areas, the interaction between the metal d-state and the G-π band has lowered the energy difference between the sp^2 and sp^3 hybridization states of the carbon atoms. As a consequence, the O_2 molecule can now form a C–O covalent bond with the graphene C atom at the sp^3 state, that weakens the O–O double bond, and brings the molecule closer to the G layer.

The adsorption geometry of the O_2 molecule on pristine graphene is parallel to the layer plane as shown in Fig. 5a with a large adsorption distance of $\sim$3 Å keeping the graphene layer practically unaltered. The reaction path involves the approach to the surface and the stretching of the molecule. In the transition state, the two oxygen atoms are placed on top positions. In the final dissociated state, oxygen atoms are located on bridge positions forming epoxy groups with a significant corrugation of the graphene layer ($\sim$0.6 Å) due to the change from the sp^2 to the sp^3 hybridization of those carbon atoms. In this case, the energy barrier increases to 3.03 eV and conversely, the undissociated molecule is 1.60 eV more stable than the decomposed state on pristine graphene, also in agreement with previous calculations.[40,41] Although this reaction could become exothermic by applying in-plane deformations larger than 5%,[41] the high reaction barrier makes this process very improbable to occur. In this case, the extra stability of the O_2 molecule arises from its magnetic behavior which is preserved after adsorption on graphene. Another important point in these calculations is related to the dissociation path, which is fairly complex: not only oxygen atoms are separated but also the G layer is being modified during the course of the reaction. The strain field induced in the graphene layer plays a crucial role in the determination of the barrier height. As an example, we found differences of a factor 2 between the complete CI-NEB calculation and a calculation approaching the path by fixing the xy position of carbon atoms and allowing relaxation only in the z axis.

Now, we turn our attention to the dissociation of the molecule on the G/Rh(111) which is substantially different from the previous case. As mentioned before, the G layer remains highly corrugated ($\sim$1 Å) on Rh(111). We separately studied the dissociation of the O_2 in the high and low areas of the moiré. Fig. 5b and c show the geometries of initial, final and transition states of both reactions. In the high parts of the moiré pattern, the dissociation path is very similar to that in free-standing graphene. The O_2 molecule adsorbs approximately parallel to the nearest graphene hexagon, with an adsorption distance of 3 Å almost identical to the free-standing G case, and its magnetic moment is preserved. The final dissociated structure shows the two oxygen atoms placed on bridge positions. The transition state is slightly different from the free-standing G case as it does not correspond exactly to on-top positions for the oxygen atoms. In spite of these structural similarities, the energetics of the process has changed significantly: the dissociation becomes exothermic – although the energy difference between the molecular and dissociated states is small, 0.20 eV, and the total barrier height is considerably reduced to 1.76 eV due to the presence of the metallic substrate.

In the low areas of the moiré pattern, where the G–metal interaction is higher, things turn even more distinct. Adsorption in the low areas leads to a stronger chemisorption binding and the partial quenching of the O_2 magnetic moment. Similarly to what occurs in bare metallic surfaces, the typical $\sim$2 μ_B of the O_2 molecule is reduced to $\sim$0.7 μ_B. The preferential adsorption configuration is completely different. The molecule adopts an on top position forming a C–O bond whose length is 1.53 Å and with a C–O–O angle of 110°. These results are in very good agreement with the sp^3 hybridization of both the central oxygen atom and the carbon atom with the formation of a simple C–O covalent bond very similar to the one observed in methanol.[42] The O–O bond length is 1.36 Å (far away from the ideal 1.21 Å of the original O_2 molecule) but compatible with the bond length of the superoxide ion.[43] In spite of a different starting configuration, the dissociation path is similar: the transition state corresponds to the dissociated atoms close to on top positions as shown in Fig. 5c. After dissociation, oxygen atoms are able to move on graphene in order to occupy even more favorable adsorption sites without finding any appreciable energy barriers. Oxygen atoms placed on top positions are able to create a C–O bond with a peculiar bond length of 1.34 Å, very large compared with double and triple bonds of CO_2 and CO molecules, but too small compared with the typical bond lengths in most organic compounds.[42] This value is only compatible with bonds created between an sp^2 carbon atom and an oxygen atom, displayed in a very reduced group of molecules like furan, conjugated esters or phenol[42] with a bond order of 1.5. In the low areas of the moiré pattern, the preferential adsorption sites are completely different from those found in the highest parts. While in the high areas oxygen atoms prefer to stay at bridge positions, in the low areas, these positions are not only less favorable but they are not even stable. Therefore, on top positions are preferred and especially those placed just over C atoms on a hollow position
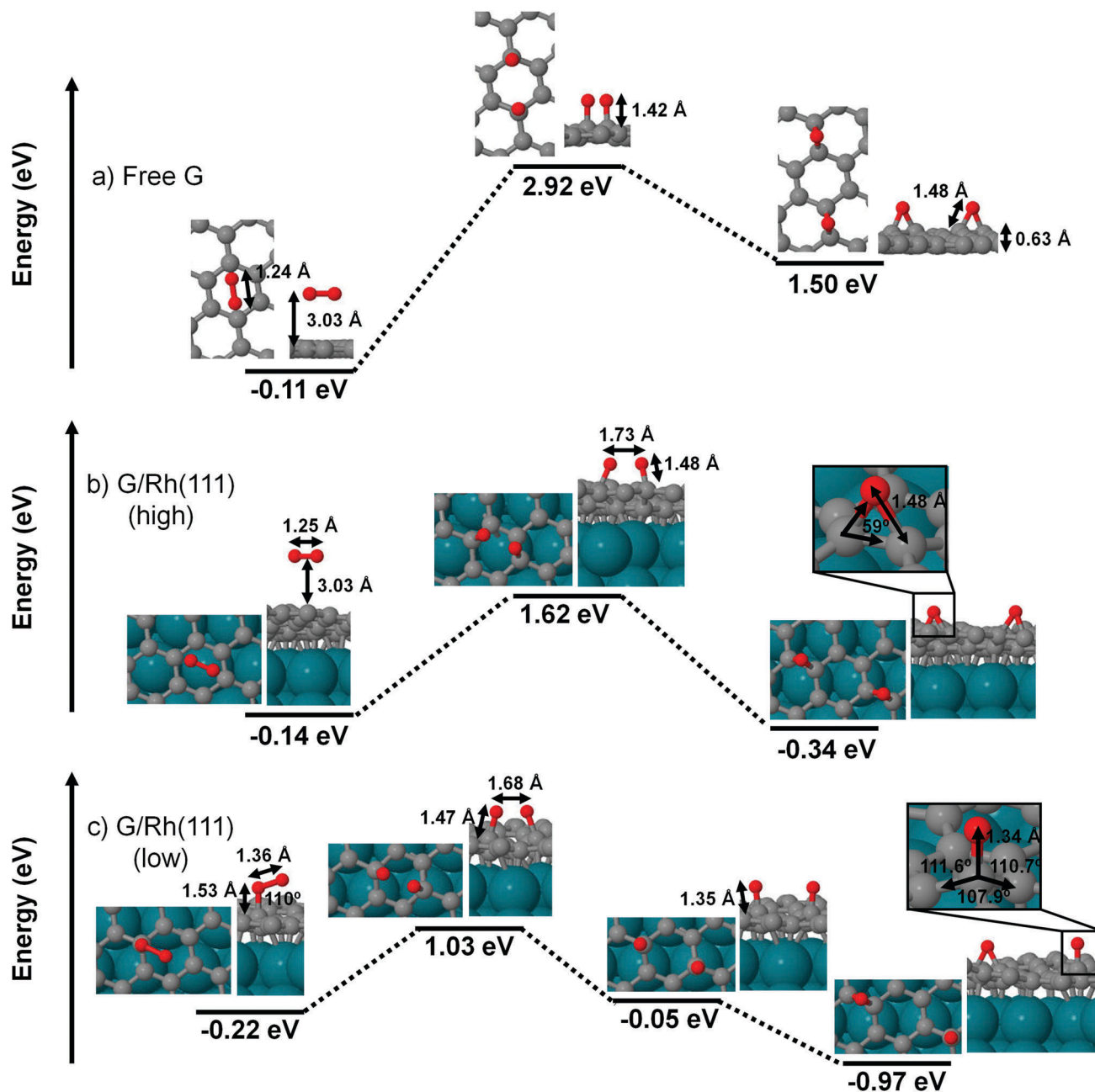
Fig. 5 Geometries of the different stages during the dissociation of molecular oxygen in (a) free standing G, (b) G/Rh(111) on a high moiré part and (c) on G/Rh(111) on a low moiré part. We show both the relative energy and the atomic structure of the initial, the final and the transition state found with the CI-NEB method. Energies are referred to the isolate G/Rh(111) slab and O_2 molecule. The color code is as follows: blue (Rh atoms), gray (C atoms) and red (O atoms).

with respect to the metallic surface. Notice that the final configuration of the molecular dissociation corresponds to an oxygen atom located on a bridge position in a mid-height region and the other placed on top just over a C atom on a hollow position of the substrate. Furthermore, in these moiré areas the energy barrier is reduced even more (1.25 eV) and the reaction is more exothermic with a difference in energy of -0.75 eV per molecule.

These results reveal a dramatic change in the G chemical activity, that goes beyond the doping-induced changes in the binding of adsorbates previously reported on G/Ir(111).[44] Our simulations show that, on the low G areas, the dissociation of small molecules like O_2 is significantly favored. This alternative mechanism for molecular dissociation on selective areas can have a significant impact on different process ranging from intercalation to covalent functionalization that involve chemical reactions with graphene. In the particular case of oxygen intercalation, there are two important factors to take into account in order to assess the relevance of this process. Firstly, the presence of small areas of the metal surface

accessible to the molecules will contribute to the O_2 dissociation with a clear preference with respect to the possible direct dissociation on top of the graphene layer,[37] since the activation energy on the metal is very small ($\sim$0.26 eV for Rh(111)). Secondly, although we have shown a clear enhancement of the catalytic activity of some regions, the feasibility of the molecular dissociation is not exclusively linked to a low energy barrier but it is also necessary to find a large enough desorption barrier for the molecular state to definitely promote the dissociation. In this case, the adsorption energy of the O_2 molecule even in the low areas of the moiré pattern is still too small to allow a systematic occurrence of this process on the interface. The adsorption energy of the oxygen molecule in free-standing graphene is -0.11 eV according to our calculations. In the presence of the Rh(111) substrate, these values are increased to -0.14 eV and -0.22 eV for the high and low areas respectively, in good agreement with previous theoretical and experimental estimations.[45] Therefore, although feasible, the experimental observation of the O_2 dissociation directly on graphene is expected to be rather difficult.

However, this result does not preclude that other molecules with higher adsorption energies could easily dissociate on G/metal systems due to the enhancement of the chemical reactivity induced by the substrate. For instance, in recent experiments carried out on G/Ru(0001), a covalent patterning of cyanomethyl radicals[46] of the low areas of the moiré was observed. In this case, a higher adhesion of this larger molecule probably allowed the direct homolytic breaking of acetonitrile on the graphene–metal interface with a very high selectivity. This successful patterning provides experimental support to the main conclusion of our theoretical results: graphene grown on highly coupled substrates displays an important enhancement of its chemical reactivity that can be exploited to tune its electronic and chemical properties.

4 Conclusions

Based on first principles calculations, we have completed a comprehensive study of the microscopic processes involved in the adsorption and diffusion of atomic oxygen on the G/Rh(111) interface and the dissociation of the O_2 molecule. Our work shows that the large G corrugation, that modulates the interaction, confers, distinctive chemical and electronic properties to the high and low areas of the moiré pattern. This fact has profound implications in the behavior of adsorbates. The adsorption is stronger in the more coupled areas due to the interaction with the substrate. In particular, the O_2 molecule displays a chemisorbed state with a partial quenching of the magnetism, similarly to what happens in catalytic metal surfaces. On the other hand, the diffusion of atomic oxygen on both the high and low areas has a energy barriers within the [0.5,1.0] eV range, although with remarkably different paths: bridge-to-bridge on the high areas *vs.* top-to-top on the low ones. Similar effects are expected in other strongly interacting metallic substrates.

Our study reveals that the G chemical properties can be substantially modified depending of the degree of coupling with the substrate, as demonstrated in the dissociation of oxygen molecule, clearly favored in the low areas of the moiré. While on the high areas of the moiré the dissociation process is similar to what happens in free-standing graphene – although with lower energy barriers, the enhanced chemical reactivity of the lower areas leads to qualitatively different dissociation paths, resembling the behaviour of molecular oxygen on metals. In fact a serious reduction of the reaction energy barrier was found, from 3.03 eV to 1.25 eV. Although the desorption barrier for the O_2 molecule might be still too high to promote a systematic dissociation on the interface, these calculations unambiguously prove the enhancement of the chemical reactivity in the graphene layer induced by the metallic substrate. So far, the introduction of defects was the only route to increase its reactivity,[8,47] and only few highly reactive species like hydrogen, fluorine and oxygen chemically attach to G. Our results show that the G–metal interaction is a versatile and powerful handle to tailor the G chemical properties and to expand the possible G applications to sensing devices.

Conflicts of interest

The authors declare no competing financial interest.

Acknowledgements

References

1 K. S. Novoselov, A. K. Geim, S. V. Morozov, D. Jiang, M. I. Katsnelson, I. V. Grigorieva, S. V. Dubonos and A. A. Firsov, *Nature*, 2005, **438**, 197.

2 K. S. Novoselov, A. K. Geim, S. V. Morozov, D. Jiang, Y. Zhang, S. V. Dubonos, I. V. Grigorieva and A. A. Firsov, *Science*, 2004, **306**, 666.

3 C. Berger, Z. Song, T. Li, X. Li, A. Y. Ogbazghi, R. Feng, Z. Dai, A. N. Marchenkov, E. H. Conrad, P. N. First and W. A. de Heer, *J. Phys. Chem. B*, 2004, **108**, 19912.

4 A. H. Castro Neto, F. Guinea, N. M. R. Peres, K. S. Novoselov and A. K. Geim, *Rev. Mod. Phys.*, 2009, **81**, 109.

5 A. A. Balandin, S. Ghosh, W. Bao, I. Calizo, D. Teweldebrhan, F. Miao and C. N. Lau, *Nano Lett.*, 2008, **8**, 902.

6 F. Bonaccorso, Z. Sun, T. Hasan and A. C. Ferrari, *Nat. Photonics*, 2010, **4**, 611.

19498 | *Phys. Chem. Chem. Phys.*, 2018, **20**, 19492–19499

This journal is © the Owner Societies 2018

7 C. Lee, X. Wei, J. W. Kysar and J. Hone, *Science*, 2008, **321**, 385.

8 F. Banhart, J. Kotakoski and A. V. Krasheninnikov, *ACS Nano*, 2011, **5**, 26.

9 H. Wang, T. Maiyalagan and X. Wang, *ACS Catal.*, 2012, **2**, 781.

10 A. T. N'Diaye, J. Coraux, T. N. Plasa, C. Busse and T. Michely, *New J. Phys.*, 2008, **10**, 043033.

11 M. M. Ugeda, D. Fernández-Torre, I. Brihuega, P. Pou, A. J. Martínez-Galera, R. Pérez and J. M. Gómez-Rodríguez, *Phys. Rev. Lett.*, 2011, **107**, 116803.

12 A. J. Martínez-Galera, I. Brihuega and J. M. Gómez-Rodríguez, *Nano Lett.*, 2011, **11**, 3576.

13 A. Martín-Recio, C. Romero-Muñiz, A. J. Martínez-Galera, P. Pou, R. Pérez and J. M. Gómez-Rodríguez, *Nanoscale*, 2015, **7**, 11300.

14 P. W. Sutter, J.-I. Flege and E. A. Sutter, *Nat. Mater.*, 2008, **7**, 406.

15 Y. S. Dedkov, M. Fonin, U. Rüdiger and C. Laubschat, *Phys. Rev. Lett.*, 2008, **100**, 107602.

16 P. Avouris and C. Dimitrakopoulos, *Mater. Today*, 2012, **15**, 86.

17 K. E. Whitener Jr. and P. E. Sheehan, *Diamond Relat. Mater.*, 2014, **46**, 25.

18 M. Batzill, *Surf. Sci. Rep.*, 2012, **67**, 83.

19 H. Tetlow, J. P. de Boer, I. J. Ford, D. D. Vvedensky, J. Coraux and L. Kantorovich, *Phys. Rep.*, 2014, **542**, 195.

20 S. Nie, N. C. Bartelt, J. M. Wofford, O. D. Dubon, K. F. McCarty and K. Thürmer, *Phys. Rev. B: Condens. Matter Mater. Phys.*, 2012, **85**, 205406.

21 R. He, L. Zhao, N. Petrone, K. S. Kim, M. Roth, J. Hone, P. Kim, A. Pasupathy and A. Pinczuk, *Nano Lett.*, 2012, **12**, 2408.

22 P. Merino, M. Švec, A. L. Pinardi, G. Otero and J. A. Martín-Gago, *ACS Nano*, 2011, **5**, 5627.

23 B. Wang, M. Caffio, C. Bromley, H. Früchtl and R. Schaub, *ACS Nano*, 2010, **4**, 5773.

24 E. Miniussi, M. Pozzo, A. Baraldi, E. Vesselli, R. R. Zhan, G. Comelli, T. O. Mentes, M. A. Niño, A. Locatelli, S. Lizzit and D. Alfè, *Phys. Rev. Lett.*, 2011, **106**, 216101.

25 S.-Y. Kwon, C. V. Ciobanu, V. Petrova, V. B. Shenoy, J. Bareño, V. Gambin, I. Petrov and S. Kodambaka, *Nano Lett.*, 2009, **9**, 3985.

26 G. Kresse and J. Furthmüller, *Phys. Rev. B: Condens. Matter Mater. Phys.*, 1996, **54**, 11169.

27 G. Kresse and D. Joubert, *Phys. Rev. B: Condens. Matter Mater. Phys.*, 1999, **59**, 1758.

28 P. E. Blöchl, *Phys. Rev. B: Condens. Matter Mater. Phys.*, 1994, **50**, 17953.

29 J. P. Perdew, K. Burke and M. Ernzerhof, *Phys. Rev. Lett.*, 1996, **77**, 3865.

30 S. Grimme, *J. Comput. Chem.*, 2006, **27**, 1787–1799.

31 D. Stradi, S. Barja, C. Díaz, M. Garnica, B. Borca, J. J. Hinarejos, D. Sánchez-Portal, M. Alcamí, A. Arnau, A. L. Vázquez de Parga, R. Miranda and F. Martín, *Phys. Rev. Lett.*, 2011, **106**, 186102.

32 J. W. Arblaster, *Platinum Met. Rev.*, 1997, **41**, 184.

33 H. J. Monkhorst and J. D. Pack, *Phys. Rev. B: Solid State*, 1976, **13**, 5188.

34 G. Henkelman and H. Jónsson, *J. Chem. Phys.*, 2000, **113**, 9978.

35 A. M. Suarez, L. R. Radovic, E. Bar-Ziv and J. O. Sofo, *Phys. Rev. Lett.*, 2011, **106**, 146802.

36 C. Romero-Muñiz, A. Martín-Recio, P. Pou, J. M. Gómez-Rodríguez and R. Pérez, *Carbon*, 2016, **101**, 129.

37 C. Romero-Muñiz, A. Martín-Recio, P. Pou, J. M. Gómez-Rodríguez and R. Pérez, *Phys. Chem. Chem. Phys.*, 2018, **20**, 13370.

38 M. Iannuzzi and J. Hütter, *Surf. Sci.*, 2011, **605**, 1360.

39 O. R. Inderwildi, D. Lebiedz, O. Deutschmann and J. Warnatz, *J. Chem. Phys.*, 2005, **122**, 034710.

40 S. Ni, Z. Li and J. Yang, *Nanoscale*, 2012, **4**, 1184.

41 M.-T. Nguyen, *J. Phys.: Condens. Matter*, 2013, **25**, 395301.

42 F. H. Allen, O. Kennard, D. G. Watson, L. Brammer, A. G. Orpen and R. Taylor, *J. Chem. Soc., Perkin Trans. 2*, 1987, S1.

43 F. A. Cotton and G. Wilkinson, *Advanced Inorganic Chemistry*, John Wiley & Sons, 3rd edn, 1972, p. 418.

44 S. Schumacher, T. O. Wehling, P. Lazić, S. Runte, D. F. Förster, C. Busse, M. Petrović, M. Kralj, S. Blügel, N. Atodiresei, V. Caciuc and T. Michely, *Nano Lett.*, 2013, **13**, 5013.

45 F. R. Bagsican, A. Winchester, S. Ghosh, X. Zhang, L. Ma, M. Wang, H. Murakami, S. Talapatra, R. Vajtai, P. M. Ajayan, J. Kono, M. Tonouchi and I. Kawayama, *Sci. Rep.*, 2017, **7**, 1774.

46 J. J. Navarro, S. Leret, F. Calleja, D. Stradi, A. Black, R. Bernardo-Gavito, M. Garnica, D. Granados, A. L. Vázquez de Parga, E. M. Pérez and R. Miranda, *Nano Lett.*, 2016, **16**, 355.

47 D. W. Boukhvalov and M. I. Katsnelson, *Nano Lett.*, 2008, **8**, 4373.

This journal is © the Owner Societies 2018

Phys. Chem. Chem. Phys., 2018, **20**, 19492–19499 | 19499